Lehrstuhl für Bildverarbeitung
Institute of Imaging & Computer Vision

Robust High-Speed Melt Pool Measurements for Laser Welding with Sputter Detection Capability

Nicolaj C. Stache and Henrik Zimmer and Jens Gedicke and Alexander Olowinsky and Til Aach

Institute of Imaging and Computer Vision
RWTH Aachen University, 52056 Aachen, Germany
tel: +49 241 80 27860, fax: +49 241 80 22200
web: www.lfb.rwth-aachen.de

in: DAGM07: 29th Annual Symposium of the German Association for Pattern Recognition. See also BibTeX entry below.

BibTeX:

```
@inproceedings{STA07b,
  author    = {Nicolaj C. Stache and Henrik Zimmer and Jens Gedicke and Alexander Olowinsky and Til Aach},
  title     = {Robust High-Speed Melt Pool Measurements for Laser Welding with Sputter Detection Capability},
  editor    = {Fred A. Hamprecht and Christoph Schn\"{o}rr and Bernd J\"{a}hne},
  booktitle = {DAGM07: 29th Annual Symposium of the German Association for Pattern Recognition},
  publisher = {Springer},
  address   = {Heidelberg},
  series    = {LNCS},
  volume    = {4713},
  month     = {Sept.\ 12--14},
  year      = {2007},
  pages     = {476--485},
  isbn      = {978-3-540-74933-2}}
```


document created on: October 30, 2008
created from file: 29.tex
cover page automatically created with CoverPage.sty
(available at your favourite CTAN mirror)

RWTH AACHEN
RHEINISCH-WESTFÄLISCHE TECHNISCHE HOCHSCHULE AACHEN

Robust High-Speed Melt Pool Measurements for Laser Welding with Sputter Detection Capability

Nicolaj C. Stache[1], Henrik Zimmer[1], Jens Gedicke[2],
Alexander Olowinsky[2], and Til Aach[1]

[1]Institute of Imaging & Computer Vision,
RWTH Aachen University, 52056 Aachen, Germany
[2]Fraunhofer Institute for Laser Technology, Steinbachstr. 15, 52074 Aachen, Germany

Abstract. Although lasers are widely used for welding in precision engineering industry, it is still a challenge to achieve high accuracy in creating and positioning welding spots at extremely high processing speed.
Towards this end, we propose a system for monitoring the welding process in order to ensure good quality of the welding spots. Our technology enables high speed image acquisition confocally to the laser beam with a direct view onto the melt. This innovative system permits accurate estimation of the melt pool's position and radius, which, however, must be performed at framerates above 200 fps. We therefore employ fast correlation based approaches for sampling the melt pool's contour and robustly fitting a circle to it. In addition, the approaches enable sputter detection via outlier classification.
To assess the performance of each presented method, extensive experiments are conducted. The proposed paradigms can furthermore be conveniently adapted to a variety of problems dealing with rapid shape estimation in noisy environments.

1 Introduction

Lasers permit to create narrow but deep weldings and they offer contact free assembling at highest processing speed – among others, these advantages have resulted in an increased use of lasers in the precision engineering industry [1]. However, a profitable use of laser welding, especially in this branch of industry, requires the generation of welding spots at high speed and with high accuracy in size and position. To meet these requirements in industrial environments, it is indispensable to monitor the laser welding process to detect flaws as early as possible. We therefore observe directly the evolution of the pool of melt caused by the laser while the laser pulse is applied. To this end, we employ a confocal laser welding system, which provides a special extension for high speed image acquisition.
The thus acquired image sequences show welding processes of copper and steel performed with a Nd:YAG laser. An additional laser is used for illuminating the

scene, which allows a direct view onto the generated melt pool without any influence of laser induced plasma. In contrast to plasma monitoring (see Fig. 1a), our direct approach dramatically improves the melt pool estimation (see Fig. 1b) and facilitates further assessment, such as sputter detection, due to the increased amount of relevant details in the images.
The images are captured with a frame rate of 5000 fps using a high-speed CMOS camera, since the welding processes last only 10 ms to 20 ms. However, the throughput of the image processing system, which is predetermined by the cycle time of the welding system (i.e. the time slot between two laser spots), has to be at least 200 fps to prevent the welding machine from stalling. At this rate the parameters, viz. radius and position of the melt pool, have to be estimated in a manner resistant to noise or sputters of the melt.
We therefore present approaches to rapidly estimate these parameters and to detect flaws via robustly fitting a circle to the melt pool's contour and perform basic error classification. For contour estimation, we utilize a novel contour sampling method via correlation of radial profiles with step edge prototypes. To infer the desired parameters from the thus sampled contour, four approaches are applied and compared. The approaches are: a completely newly designed method, adapted types of the Hough Transform, Least Median of Squares regression, and RANSAC (RANdom SAmple Consensus).
Recent experiments have shown that the main ideas presented here can be conveniently adapted to various estimation problems such as fast position recognition of bearings in industrial vision and cell recognition for early cancer diagnosis.
The paper is organized as follows: First, our welding and image acquisition system is described. Second, the algorithms for melt pool parameter estimation are introduced. Then, the results of extensive experiments are presented and comparisons of the algorithms are made. The paper concludes with a discussion and an outlook for ongoing work.

2 Welding and Image Acquisition System

Unlike other approaches, which use the radiation of the laser induced plasma for process monitoring with a spatially integrating photo detector (often a photo diode), we employ a special setup which allows the acquisition of 2D images confocally with the laser. This setup is known as *Coaxial Process Control*-system (CPC-system) [4], [5]. Compared to a photo diode system, the CPC-system, when equipped with a high speed camera, provides image data with much more relevant information for the welding process, and a strongly increased resolution.
To obtain melt pool images without being disturbed by plasma radiation, we extended the basic CPC-system, which is composed of a Nd:YAG laser, a dichroit and a camera, see Fig. 2. As illustrated, the Nd:YAG laser partly shares its optical path with the camera. This is implemented via the dichroit, which reflects the laser wavelength but is transparent for the wavelengths the camera should capture. With only this basic CPC setup, however, the camera would capture the radiation of the laser induced plasma, which prevents a direct view onto the

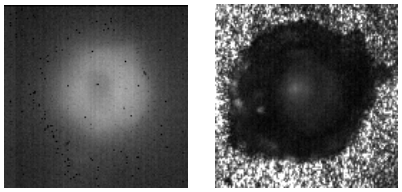

Fig. 1. Frames of a welding sequence: (a) Meltpool without additional illumination (b) with additional illumination – direct view onto the melt pool.

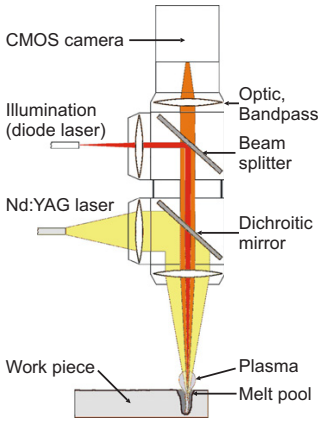

Fig. 2. Welding system with extension for image acquisition and additional illumination [5].

melt.

To cope with this problem, we extended the setup by using a second beam splitter in front of the camera, which introduces an additional illumination from a diode laser with a wavelength of 830 nm. Additionally, we place an appropriate bandpass filter in front of the camera. The passband of this bandpass is tuned to a small band around 830 nm, where the radiation emitted by the plasma is close to zero. This means, in turn, that the plasma is translucent in this small band and, therefore, we obtain the desired direct view onto the melt pool shown in Fig. 1b).

3 Parameter Estimation

This section describes several techniques for estimating the radii and positions of the melt pools in the image sequences. We concentrate on approaches which use information about the melt pool's contour and fit a circle to estimate radius and position. The advantage of this contour-based method over blob based approaches and derivatives based on matching of entire melt pool frames with sets of prototypes [7], is the higher achievable throughput and the possibility for localizing defects such as sputters in the contour. Conventional approaches, working on entire images, such as the standard Hough Transform [3] are computationally far too expensive. In contrast to the Hough Transform, high throughput can be obtained with the computationally inexpensive fast boundary point analysis in [7] but the robustness of this method to outliers is weak.

To comply with both throughput and robustness constraints, we first estimate contour points, and then robustly fit a circle to these points. Since there are various approaches for robust fitting [6], [3], [8], a rigorous comparison, as mentioned in the introduction, is made.

3.1 Contour Point Estimation

The starting point for the algorithms – except for the Hough Transform, which operates on correlation values – are the points extracted from the melt pool's contour. To estimate these points with low computational effort, we consider n radial profiles of the melt pool images and correlate each profile with a precomputed set of step edges. The positions of the radial profiles for $n = 8$ are highlighted in Fig. 3.

Before the correlations are computed, both the step edges and the profiles have

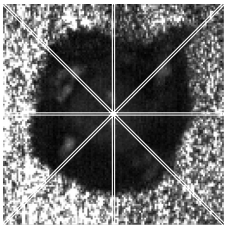

Fig. 3. Melpool with highlighted positions of eight radial profiles.

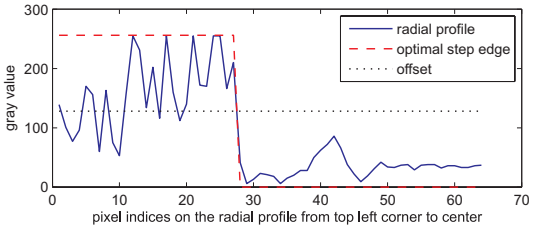

Fig. 4. Radial profile of the top left corner with estimated step edge referring to the sought contour point. Dotted line: Offset which has to be compensated with a gray value shift.

to be freed from their offsets which results in a shift of the gray values. With this operation, the gray values corresponding to the melt pool pixels become negative and the background values become positive. It is important that the symmetry of these values in the radial profile is roughly identical with the symmetry in the precomputed step edges to yield a high accuracy in estimating the edge's position. This leads to a normalization by subtracting the gray value offset. Normalization is followed by correlation computation, which we conveniently implemented as a matrix multiplication. This is similar to linear convolution via multiplication with a Toeplitz matrix and can be described as

$$\mathbf{y} = \mathbf{H} \cdot \mathbf{x} \,, \tag{1}$$

where $\mathbf{y}$ denotes the correlation vector, $\mathbf{H}$ is the Toeplitz-Matrix, which is composed of the precomputed step edge prototypes and $\mathbf{x}$ represents the gray values of the radial profile. An example with idealized $\mathbf{x}$ is

$$\underbrace{\begin{pmatrix} 2 \\ 4 \\ 2 \\ 0 \\ -2 \end{pmatrix}}_{\mathbf{y}} = \underbrace{\begin{pmatrix} 1 & 1 & 1 & 1 \\ -1 & 1 & 1 & 1 \\ -1 & -1 & 1 & 1 \\ -1 & -1 & -1 & 1 \\ -1 & -1 & -1 & -1 \end{pmatrix}}_{\mathbf{H}} \cdot \underbrace{\begin{pmatrix} -1 \\ 1 \\ 1 \\ 1 \end{pmatrix}}_{\mathbf{x}} \,. \tag{2}$$

As can be seen, the precomputed step prototypes are stacked in $\mathbf{H}$, which, with these ideal models, degenerates to a triangular matrix. Obviously, the second line in $\mathbf{H}$ fits best to $\mathbf{x}$ – consequently, the second entry in $\mathbf{y}$ exhibits the maximum value. The corresponding contour point can now be determined via the position of the maximum value in $\mathbf{y}$.
The challenge in estimating contour points this way is to accurately estimate the gray value offset for normalization because its value varies from frame to frame. We therefore implemented a normalization method by computing the offsets as the mean values of the profiles and the step edges. Thus, these offsets adapt to brightness variations and are insensitive to noise e.g. resulting from bad pixels in the camera's sensor. However, the increased adaptivity and robustness result in the loss of the triangular form of $\mathbf{H}$.

3.2 Robust Fitting Algorithms

The contour sampling described above is highly robust to noise because always entire profiles are correlated. However, the obtained contour points are still influenced by sputters or bright reflections in the melt, which should not degrade the melt pool parameter estimation. Therefore, a robust fitting of the circle model with these detected points is vital. We address this challenging task by developing a new approach called "Least Distances (L. Dist.)" and by adapting three widely used paradigms for robust regression to the problem at hand.

Least Distances ("L. Dist.") Compared to the techniques, to be introduced in the following, this approach is closest tailored to the problem stated above, since it uses the highest degree of prior knowledge about the welding process for fitting and rejecting outliers.
Our algorithm is based on the fact that the material to be welded melts continuously. Consequently, the melt pool's radius increases smoothly over successive frames. Thus, undisturbed contour points are distinguished from those disturbed by, e.g., sputter, by evaluating the distance of each contour point to the preceding circle. With this approach we thus make use of the temporal dependencies between the melt pool's parameters of successive frames, due to the physics of welding.
The trusted contour points, chosen by this method and used for circle fitting, are those $m_t = n/2$ points (n = number of contour points, $n \geq 8$), which have the smallest Euclidean distance to the preceding circle. However, to ensure that the trusted points are reasonably distributed, the contour is divided into four quadrants and from each quadrant, at least one point (namely the point with the smallest distance) is selected. This procedure should help to better cope with melt pools which are not perfectly round.
After contour point selection, the circle is fitted via Least Mean Squares to the m_t trusted points.

Hough Transform The common ground of "L. Dist." (and the following methods) is the attempt of fitting a circle to contour points extracted first. Thus, only the *maxima* of the correlation vectors $\mathbf{y}$ in (1) are considered, since they represent the points where the contour most likely is to be. However, the strengths of these maxima and the existence of secondary maxima are not considered. These downsides can be addressed by the Hough Transform [3] for finding the circle, whose contour points maximize the correlation in sum over all contour points. As mentioned before, on our current platform (2.66 GHz, Intel Core2Duo PC), the standard Hough Transform (denoted by "Hough Ext.") can not comply with the stringent real time constraints. Its performance is in the following therefore provided more as a reference. However, the limited number of correlation vectors $\mathbf{y}$, the possibility to eventually shrink the Hough accumulator space by invoking additional prior knowledge, and the possibility of further speedup via a lookup table for the pixels to be accumulated, make it an earnest alternative candidate for our application. We thus implemented a trimmed-down and accelerated version, called "Hough Ltd." which inherently makes use of the temporal dependencies described in 3.2 by utilizing the previously estimated circle parameters as initial guess for defining a small sliding search space around these.

RANSAC The most commonly used approach for robust fitting in industrial vision is RANSAC, introduced by Fishler and Bolles [2]. Unlike "Hough Ltd." or "L. Dist", RANSAC solely uses the given shape model for outlier rejection. For the problem at hand, we implemented RANSAC with the following steps:

1. Select a set of $p = 3$ contour points randomly (three points are required to determine a circle),
2. Construct a circle through these,
3. Count the number of points which lie within an error tolerance of $\epsilon_{\max}$ to the circle (so-called inliers),
4. If the number of inliers is greater than some threshold $n_{\min}$, do least squares circle fitting for all inliers, else repeat the above process, i.e. start again at 1., until a maximum number $m_{\max}$ of trials is reached.

Least Median of Squares Slightly different to RANSAC, but as well solely based on the shape model, is Least Median of Squares Regression (LMedS), which solves the nonlinear minimization problem

$$\min \underset{i}{\operatorname{med}} r_i^2 \ , \tag{3}$$

where r_i^2 denotes the squared residual, i.e. the squared distance of the remaining contour points to the fitted circle. Although (3) looks very similar to Least Mean Squares regression, a closed form solution of this expression is not available. Thus, LMedS has to perform a search in the space of possible estimates generated from data. The procedure we implemented for n given points is composed of the following steps [8]:

1. Draw m random subsamples of $p = 3$ different points,
2. Construct circles through the points of the subsamples,
3. Determine the median of the squared residuals for each circle,
4. Pick the circle yielding the smallest median,
5. Consider the distance of all points to the picked circle and reject points with distances $> t$,
6. Fit a circle via least mean squares with the remaining points.

In contrast to Least Mean Squares, LMedS can resist the effect of 50% of gross outliers in data. Step 5 and 6 help to compensate the poor efficiency of LMedS in the presence of Gaussian noise. According to Rousseeuw in [6], t calculates to

$$t = M \left(3.7065 + \frac{18.5325}{n-p}\right)^2 , \tag{4}$$

where M denotes the minimal median.

4 Results

This section presents the performances and error rates of the described algorithms compared with a hand selected ground truth. The algorithms were coded in Matlab and executed on a standard PC (Intel Core2Duo, 2.66 GHz, 2 GB RAM). The database for evaluation contains approximately 1020 frames (and the corresponding ground truths) taken from 12 different welding sequences of copper and steel. As mentioned in the introduction, these sequences are recorded with a high-speed camera with 128 × 128 pixels at 5000 fps. The welding is performed with a Nd:YAG Laser (1064 nm wavelength) and the scene is confocally illuminated with a diode laser (830 nm wavelength). All the presented images exhibit a field of view of 0.8 × 0.8 mm^2.
To assess the algorithms for both sequences with well-behaved melt pools and sequences with high defect rates (due to sputters and reflections, see Fig. 6) separately, each of these is split into two parts. The first part typically exhibits well-behaved melt pools and the second part exhibits higher defect rates – it can be observed that the defect rate increases with the radius, which in turn increases with the frame number and time, see Fig. 6.
For comparison, the error rates ϵ_1, ϵ_2, and ϵ are computed from the areas in pixels, which are correctly or incorrectly classified by the algorithms compared with ground truths. More specifically, ϵ_1 is the probability of background pixels which are misclassified as melt pool pixels ("false positive rate"), ϵ_2 is the probability of the melt pool pixels being misclassified as background ("false negative rate"), and ϵ is the total error rate.
The settings of the algorithms, used for obtaining the following results, are listed in Tab. 1. All settings are carefully chosen to yield reasonable results with the algorithms. In case of LMedS, m is specified to ensure that the probability of drawing at least one completely undisturbed combination is 99% in the presence of 50% disturbed contour points. The results obtained with these settings are

depicted in Tab. 2 and Fig. 5.
As can be observed, the two approaches, viz. "L. Dist." and "Hough Ltd.", exploiting temporal dependencies due to the continuity in melt pool changes, perform better than the other approaches and yield moderate error rates. However, among these two, "L. Dist." exhibits higher throughput while "Hough Ltd." is slightly better in total error rate ϵ. The error rates depicted in Tab. 2 might, however, be further improved by optimizing the normalization described in section 3.1, because the algorithms tend to overestimate the size of the melt pools (ϵ_1 is greater than ϵ_2 – see Tab. 2).

Global setting	$n = 16$	number of radial profiles
RANSAC	$p = 3$	initial set of points
	$\epsilon_{\max} = 4$ pix.	error tolerance for inliers
	$n_{\min} = 4$	minimum number of inliers
	$m_{\max} = 80$	maximum number of trials
LMedS	$p = 3$	initial set of points
	$m = 44$	number of initial subsamples
L. Dist.	$m_t = 8$	number of trusted points
Hough Ext.	$s(y, x, r) = 64^{+8}_{-8},\ 64^{+8}_{-8},\ 5^{+72}_{0}$	search space in y, x, r direction
Hough Ltd.	$s(y, x, r) = i_y^{+2}_{-2},\ i_x^{+2}_{-2},\ i_r^{+5}_{-5}$	search space
	$i_y,\ i_x,\ i_r$	parameters of preceding circle (first initialized with: 64, 64, 15)

Table 1. Global settings for the different robust fitting algorithms.

Algorithm	Part	ϵ_1	ϵ_2	ϵ	fps
RANSAC	1	8.2	1.5	6.1	446.3
	2	12.5	2.2	8.3	442.9
LMedS	1	6.8	0.7	4.9	220.9
	2	10.8	1.1	6.8	221.0
L. Dist.	1	5.0	2.0	4.1	1084.3
	2	8.3	1.8	5.7	1084.2
Hough Ext.	1	5.2	0.7	3.8	39.6
	2	10.3	0.9	6.3	39.6
Hough Ltd.	1	5.0	4.8	4.2	867.5
	2	8.6	0.7	5.5	867.7

Table 2. Results for the different robust fitting algorithms ('Part' refers to the splitting of the sequences into two parts, ϵ_1 = false positive rate in %, ϵ_2 = false negative rate in %, ϵ = total error rate in %, fps = frames per second with a 2.66 GHz Core2Duo, Matlab code).

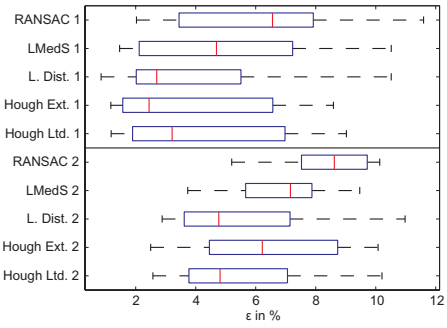

Fig. 5. Boxplot of the total error rate for both sequence parts ("RANSAC 1" e.g. indicates the error rates for part 1 of the sequences, obtained with RANSAC). The lines in the boxes mark the medians, the boxes encompass the two inner quartiles of the quantity of results, whereas the "whiskers" and crosses mark the two remaining outer quartiles.

4.1 Edge model improvement and sputter detection

In case of severe disturbances due to reflections in the melt, the edge model offers the possibility for further improvement. Fig. 6, row a) shows detected contour points with the standard edge model – it can be observed that some contour points are disturbed by reflections in the melt. However, most of these reflections arise in the inner parts and not on the periphery of the melt pools. Consequently, a small (dark) rim of molten material between reflection and background remains. This can be exploited by adapting the precomputed edge prototypes, which is straightforwardly done by inserting stripes of zeros, which cover the inner melt pool region, into the prototypes. As a consequence, the inner parts of the melt pool no longer count for correlation and thus, reflections in these parts no longer disturb the melt pool estimation (see Fig. 6 row b)).
In addition to melt pool estimation, the contour based approach offers the benefit for sputter detection without major effort. A sputter is simply recognized as a contour point lying beyond a threshold distance d_t outside the fitted circle. Fig. 6 (see sputter points) shows an example for melt pool estimation with "L. Dist." and sputter detection ($d_t \geq 4$ pixels like in RANSAC). The accuracy of sputter detection may be increased by detecting more contour points, which of course decreases the detection rate. However, "L. Dist." still yields a throughput of 338 fps with $n = 60$ radial profiles.

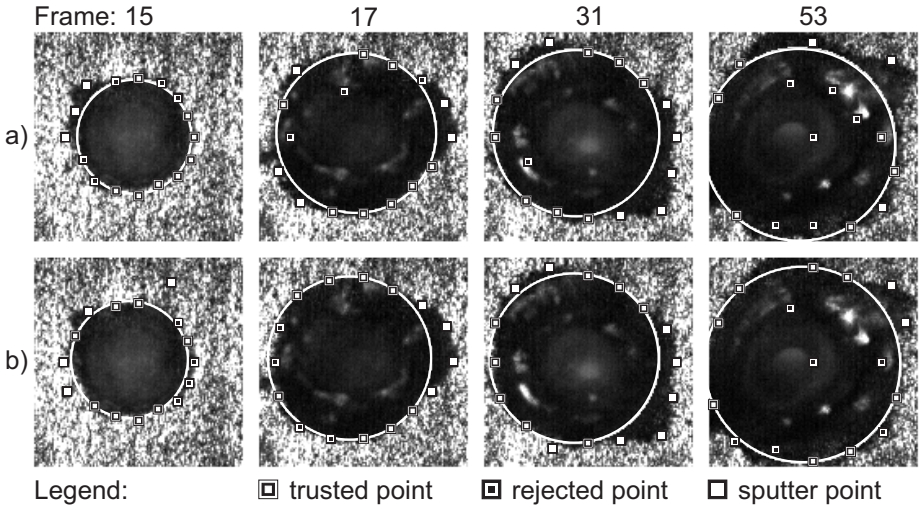

Fig. 6. Melt pool evolution during a welding process of copper. The contour points and circles are obtained with "L. Dist.". Row a): contour points obtained with idealized edge prototypes, row b): contour points and circles obtained with an initial additional stripe of zeros in the edge prototypes.

5 Conclusions

We presented approaches for process monitoring in laser welding via high speed and robust estimation of melt pool parameters. To this end, we employed a special setup with confocal illumination and a bandpass filter in front of the camera to acquire images without influence of plasma radiation. The obtained images thus allow the desired parameter estimation.
All approaches presented in this contribution are based on contour sampling via correlation of step edge prototypes with radial profiles of the images. This sampling is followed by parameter estimation, where two approaches, which use process-pertinent knowledge achieve the best performance. The main ideas of these algorithms can be easily adapted to other industrial and medical vision tasks as recent experiments have shown.
Our ongoing work is on the extension of the algorithms towards an increased robustness to discontinuities in the background e.g. caused by adjacent melt pools which, in turn, paves the way for monitoring of welding seams.

Acknowledgments

The authors thank Dipl.-Ing. Boris Regaard, Fraunhofer ILT who kindly provided the welding sequences used in this paper.
This work is funded by the collaborative research project "INTAKT" in the funding program "InnoNet" from the German Federal Ministry of Economics and Technology (BMWi) with VDI/VDE-IT. The authors gratefully acknowledge this support as well as the active cooperation of all project partners.

References

1. A. Bollig, S. Mann, R. Beck, S. Kaierle. Einsatz optischer Technologien zur Regelung von Laserstrahlschweißprozessen. *Automatisierungstechnik*, 53:513–521, 2005.
2. M. A. Fischler, R. C. Bolles. Random sample consensus: a paradigm for model fitting with applications to image analysis and automated cartography. *Commun. ACM*, 24(6):381–395, 1981.
3. P. V. C. Hough, A. Arbor. Method and means for recognizing complex patterns. *United States Patent and Trademark Office*, 3069654, 1962.
4. C. Kratzsch. *Realisierung eines kamerabasierten Prozessüberwachungssystems am Beispiel des Laserstrahlschweißens.* PhD thesis, RWTH Aachen, 2003.
5. B. Regaard, S. Kaierle, W. Schulz, A. Moalem. Advantages of Coaxial External Illumination for Monitoring and Control of Laser Materials Processing. *ICALEO*, pp. 915–919, 2005.
6. J. Rousseeuw, Peter and M. Leroy, Annick. *Robust Regression and Outlier Detection.* John Wiley & Sons, New York, 1987.
7. N. C. Stache, H. Zimmer, J. Gedicke, B. Regaard, A. Olowinsky, A. Knepper, T. Aach. Approaches for high-speed melt pool detection in laser welding applications. *Proc. VMV 2006*, pp. 217–224, 2006.
8. Z. Zhang. Parameter estimation techniques: A tutorial with application to conic fitting. Technical Report RR-2676, INRIA, 1997.